Available online at www.sciencedirect.com
SCIENCE DIRECT®
International Journal of Mass Spectrometry 227 (2003) 205–216
International Journal of Mass Spectrometry
www.elsevier.com/locate/ijms

3-Dimensional structural characterization of cationized polyhedral oligomeric silsesquioxanes (POSS) with styryl and phenylethyl capping agents

Erin Shammel Baker, Jennifer Gidden, David P. Fee, Paul R. Kemper, Stanley E. Anderson[1], Michael T. Bowers*

Department of Chemistry & Biochemistry, University of California, Santa Barbara, CA 93106, USA

Received 6 December 2002; accepted 23 January 2003

Abstract

The 3-dimensional gas-phase conformations of polyhedral oligomeric silsesquioxanes (POSS), $R_8Si_8O_{12}$, capped with styryl and phenylethyl substituents (R) and cationized by sodium were examined. MALDI was used to generate sodiated styryl–POSS ($Na^+Sty_8T_8$) and phenylethyl–POSS ($Na^+PhEt_8T_8$) ions and their collision cross-sections in helium were measured using ion mobility-based methods. Five distinct conformers with different collision cross-sections were experimentally observed for $Na^+Sty_8T_8$ while only one conformer was detected for $Na^+PhEt_8T_8$. Theoretical modeling of $Na^+Sty_8T_8$, using molecular mechanics/dynamics calculations, predicts three low-energy conformations. In each conformer, the Na^+ ion binds to four oxygens on one side of the Si–O cage and the styryl groups extend away from the cage. However, different numbers of styryl groups "pair" together (forming 2, 3 or 4 pairs), yielding three different conformations. The calculated cross-sections of these conformers match the largest three cross-sections obtained from the ion mobility experiments (∼2% error). If, however, one or two of the styryl groups are rotated so that the phenyl groups are "*cis*" with respect to the Si atom on the cage (i.e., the Si–C=C–C dihedral angle changes from 180 to 0°) two smaller conformers are predicted by theory whose cross-sections match the smallest two values obtained from the ion mobility experiments (1–2% error). Theoretical modeling of $Na^+PhEt_8T_8$ yields one low-energy conformation in which the Na^+ ion binds to one oxygen on the Si–O cage and is sandwiched between two phenyl groups. The remaining phenylethyl groups fold toward the Si–O cage, yielding a significantly more compact structure than $Na^+Sty_8T_8$ (∼20% smaller cross-section). The calculated cross-section of the predicted $Na^+PhEt_8T_8$ structure agrees very well with the experimental cross-section obtained from the ion mobility experiments (∼1% error).

Keywords: Capping agents; Dynamics; Reflectron

1. Introduction

Polyhedral oligomeric silsesquioxanes (POSS) are a class of materials with a wide range of applications from polymer modifiers to lubricants [1,2]. A sturdy silicon–oxygen framework of the form $(RSiO_{3/2})_n$, where R is an organic substituent or cap, makes up

* Corresponding author. Tel.: +1-805-893-2893; fax: +1-805-893-8703.
E-mail address: bowers@chem.ucsb.edu (M.T. Bowers).
[1] Department of Chemistry, Westmont College, Santa Barbara, CA 93108, USA.

1387-3806/03/$ – see front matter © 2003 Elsevier Science B.V. All rights reserved.
doi:10.1016/S1387-3806(03)00068-X

the internal structure of these compounds. The most common POSS structures added to synthetic polymers are in the form of a hollow cage with stoichiometry $R_8Si_8O_{12}$ (R_8T_8). The cage is approximately cubic with silicon atoms at the corners, oxygen atoms bridging each Si atom, and capping agents such as esters, epoxies, methacrylates, siloxanes, or nitriles at the eight Si vertices. The resulting compounds can be incorporated into traditional polymer systems to give significant improvements in both physical and thermal properties [3–5].

Recent studies on POSS have focused on synthesizing select POSS monomers with particular substituent groups (R) that can be easily grafted into polymeric materials and yield the desired physical and chemical improvements. In these studies, it is important to be able to quickly and accurately characterize the size, shape, and functionality of the new POSS monomers (as well as understand how this structure and functionality of POSS affects the polymer structure and properties). Traditional spectroscopic techniques such as NMR and X-ray crystallography are usually used to characterize these systems but they can often yield only averaged conformational data. We have developed methods based on mass spectrometry and ion mobility that can give detailed information about the conformations of large molecules in the gas phase.

Ion mobility [6,7] is determined by measuring the time required for a mass-selected ion to drift a given distance through a buffer gas under the influence of a weak electric field. This drift time is directly related to the conformation the ion exhibits. Ions with smaller collision cross-sections (more compact structures) arrive at the detector faster than ions with larger collision cross-sections (less compact structures). In order to interpret the experimental cross-sections in terms of actual detailed structures, computational methods are used to generate theoretical structures and cross-sections for the POSS molecules to compare with the experimentally determined cross-sections. Our initial work on applying ion mobility methods to examine the structures of various POSS compounds with different substituents has been published [8]. Good agreement between cross-sections obtained from ion mobility measurements and those calculated for X-ray and theoretical structures was observed. In this paper we report on the application of ion mobility to the structural analysis of two closely related POSS monomers with styryl (Sty) and phenylethyl (PhEt) substituent groups.

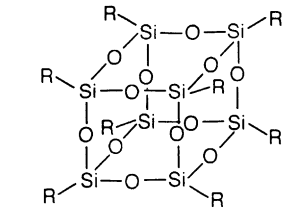

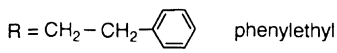

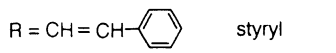

These two substituents differ only by the types of carbons connected to the Si–O cage: $–CH_2–CH_2–$ vs. –CH=CH–. Sodiated styryl–POSS ($Na^+Sty_8T_8$) and phenylethyl–POSS ($Na^+PhEt_8T_8$) ions were generated by MALDI and their collision cross-sections measured using ion mobility methods and theoretical modeling. An X-ray crystallography structure was available for Sty_8T_8 and its calculated collision cross-section was also compared to the cross-sections obtained from the ion mobility measurements and theoretical modeling.

2. Experiment

Experiments were performed using a home-built MALDI-TOF instrument shown in Fig. 1. 2,5-Dihydroxybenzoic acid (DHB) dissolved in methanol to a concentration of 100 mg/mL was used as the matrix. The styryl–POSS (Sty_8T_8) and phenylethyl–POSS ($PhEt_8T_8$) compounds were also dissolved in methanol to a concentration of 1 mg/mL each. A saturated solution of NaI dissolved in methanol was used as the cationizing agent. Approximately 8 μL of the NaI solution was mixed with 50 μL of the DHB solution and 50 μL of one of the POSS solutions and applied to a 2.8 cm section of a stainless steel cylindrical rod

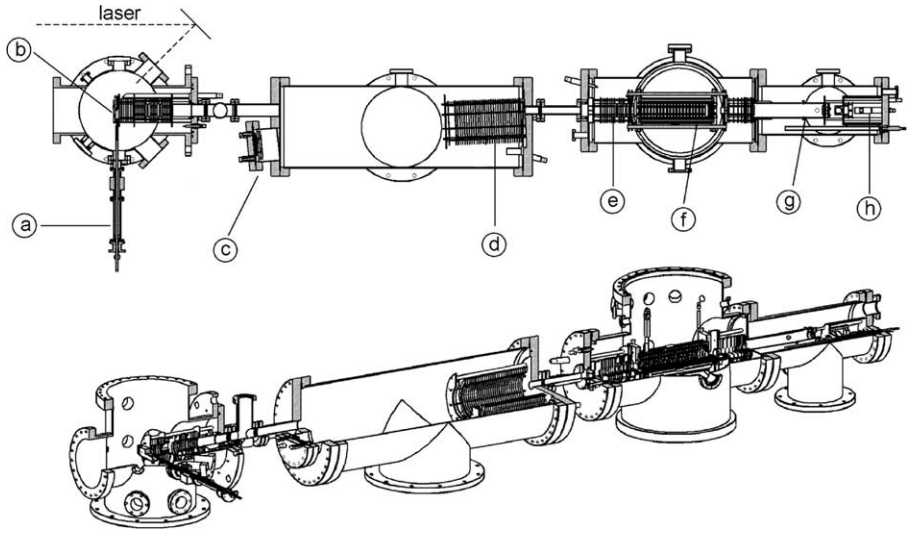

Fig. 1. Schematic of the overall instrument used in this study. (a) Sample probe; (b) sample inside the MALDI source; (c) detector used when the TOF is operated in reflectron mode; (d) reflectron; (e) deceleration lenses; (f) drift cell; (g) quadrupole; (h) detector used for the ion mobility experiments.

(1.27 cm in diameter) and dried. The sample is inserted into the MALDI source and a stepper motor rotates and translates the stainless steel rod, exposing fresh areas of sample to the laser. A nitrogen laser (Lasertechnik Berlin MSG 400, $\lambda = 337$ nm) is used to desorb and ionize the sample. The laser is usually operated at 30 Hz and has a pulse width of $\leq$10 ns and a maximum average power of 12 mW. The ions are desorbed into a two-section (Wiley-McLaren) ion source and accelerated down a 1 m long flight tube with a pulsed 9 kV acceleration voltage. The MALDI-TOF is operated in reflectron mode to obtain high-resolution mass spectra of the ions formed in the source.

For the ion mobility experiments, the reflectron is turned off and a linear mass gate is turned on, allowing the ions to travel through to the drift cell. In order to prevent collision-induced dissociation, the ions are decelerated to ~300 eV before they are focused into the 0.5 mm entrance orifice of the drift cell. The 20-cm long cylindrical glass drift cell is filled with ~1.5 Torr of helium gas. Twenty drift guard rings are spaced evenly throughout the cell to provide a uniform electric field across the cell. The cell temperature is most often kept at 300 K for initial experiments but can be varied from 90 to $\geq$500 K depending on experimental needs. After exiting the drift cell through another 0.5 mm orifice, the ions are gently accelerated through a quadrupole mass filter and detected with an electron multiplier. The quadrupole is set to a specific mass-to-charge ratio (*m/z*) to eliminate any ions that might arise from fragmentation in the drift cell and interfere with mobility measurements. The pulsed source extraction voltage triggers a timing sequence so that the ions are detected as a function of time, yielding an arrival time distribution (ATD). This ATD is collected on a multi-channel scalar with a 5-μs time resolution. The mobility, K_o, of the ions is accurately determined from a series of ATDs measured at different voltages across the drift cell (7.5–16 V/cm). Using kinetic theory, the ion's collision cross-section can also be determined.

2.1. Data analysis

The reduced mobility of the mass-selected ions can be obtained from the ATD using Eq. (1) [9]:

$$K_o = \left(l^2 \frac{273}{760T} \frac{p}{V} \frac{1}{t_A - t_o} \right) \quad (1)$$

where l is the length of the cell, T the temperature in K, p the pressure of the He gas (in Torr), V the strength of the electric field, t_A the ions' arrival time taken from the center of the ATD peak, and t_o is the amount of time the ion spends outside the drift cell before reaching the detector. A series of arrival times (t_A) are measured by changing the voltage (V) applied to the drift cell. A plot of t_A vs. p/V yields a straight line with a slope inversely proportional to K_o and an intercept of t_o. Once K_o is known, the ion's collision cross-section can be obtained using Eq. (2):

$$\Omega^{(1,1)} = \frac{3e}{16N_o}\left(\frac{2\pi}{\mu k_b T}\right)^{1/2}\frac{1}{K_o} \quad (2)$$

where e is the charge of the ion, N_o the number density of He at STP, T the temperature, k_b the Boltzmann's constant, and μ is the ion–He reduced mass [9].

2.2. Theoretical modeling

Conformational details about the POSS ions are obtained by comparing the experimental cross-sections determined from the ATDs to the cross-sections of theoretical structures. For large molecules like these POSS systems, molecular mechanics/dynamics methods are needed to generate the trial structures. We have had success in using the AMBER set of molecular mechanics/dynamics programs [10] to provide reliable structures of many synthetic polymers [11–15]. In these cases, the theoretical cross-sections agreed well with the ion mobility data. Unfortunately, the AMBER force field is not parameterized for Si-containing compounds such as POSS. Therefore, published ab initio calculations by Sun and Rigby [16], designed to provide siloxane parameters for a CFF-type force field, were used to develop the necessary Si parameters needed in the AMBER database. These parameters were tested for a number of POSS compounds with different Si–O cage sizes and R substituents [8]. The cross-sections of the AMBER-generated structures agreed very well with cross-sections obtained for known X-ray structures and from the ion mobility measurements.

Using the appropriate AMBER parameters, trial structures were calculated for $Na^+Sty_8T_8$ and $Na^+PhEt_8T_8$. An annealing/energy minimization cycle was used to generate 100 low-energy structures for $Na^+Sty_8T_8$ and $Na^+PhEt_8T_8$. In this cycle, an initial minimization of the structure is followed by 30 ps of molecular dynamics at 800 K and 10 ps of molecular dynamics in which the temperature is incrementally dropped to 0 K. The resulting structure is then energy minimized again and used as the initial structure for another minimization/dynamics run. After 100 low-energy structures are obtained, their cross-sections must be calculated for comparison with experimental cross-sections. A temperature-dependent projection model [17,18], with appropriate atomic collision radii calculated from the ion–He interaction potential, is used to calculate the angle-averaged collision cross-section of each theoretical structure. From this data, a scatter plot of cross-section vs. energy for the 100 minimized structures is collected and used to help identify the ions observed in the experimental ATDs.

3. Results/discussion

MALDI-TOF mass spectra of Sty_8T_8 and $PhEt_8T_8$ doped with NaI are shown in Fig. 2. No fragmentation occurs for either POSS compound (the peaks below m/z 400 are due to the matrix and salt). Only sodiated POSS ions, $Na^+Sty_8T_8$ (m/z 1263) and $Na^+PhEt_8T_8$ (m/z 1279), are observed in the mass spectra regardless of whether NaI is added to the sample. For the ion mobility experiments, $Na^+Sty_8T_8$ or $Na^+PhEt_8T_8$ ions are gently injected into the drift cell and their ATDs collected. Fig. 3 shows typical ATDs obtained for $Na^+Sty_8T_8$ (Fig. 3a) and $Na^+PhEt_8T_8$ (Fig. 3b) at a drift cell temperature of 300 K.

3.1. $Na^+Sty_8T_8$

Five resolvable peaks appear in the $Na^+Sty_8T_8$ ATD, indicating five distinct conformers are present which have different mobilities (and hence drift times). The shape of the ATD did not change with

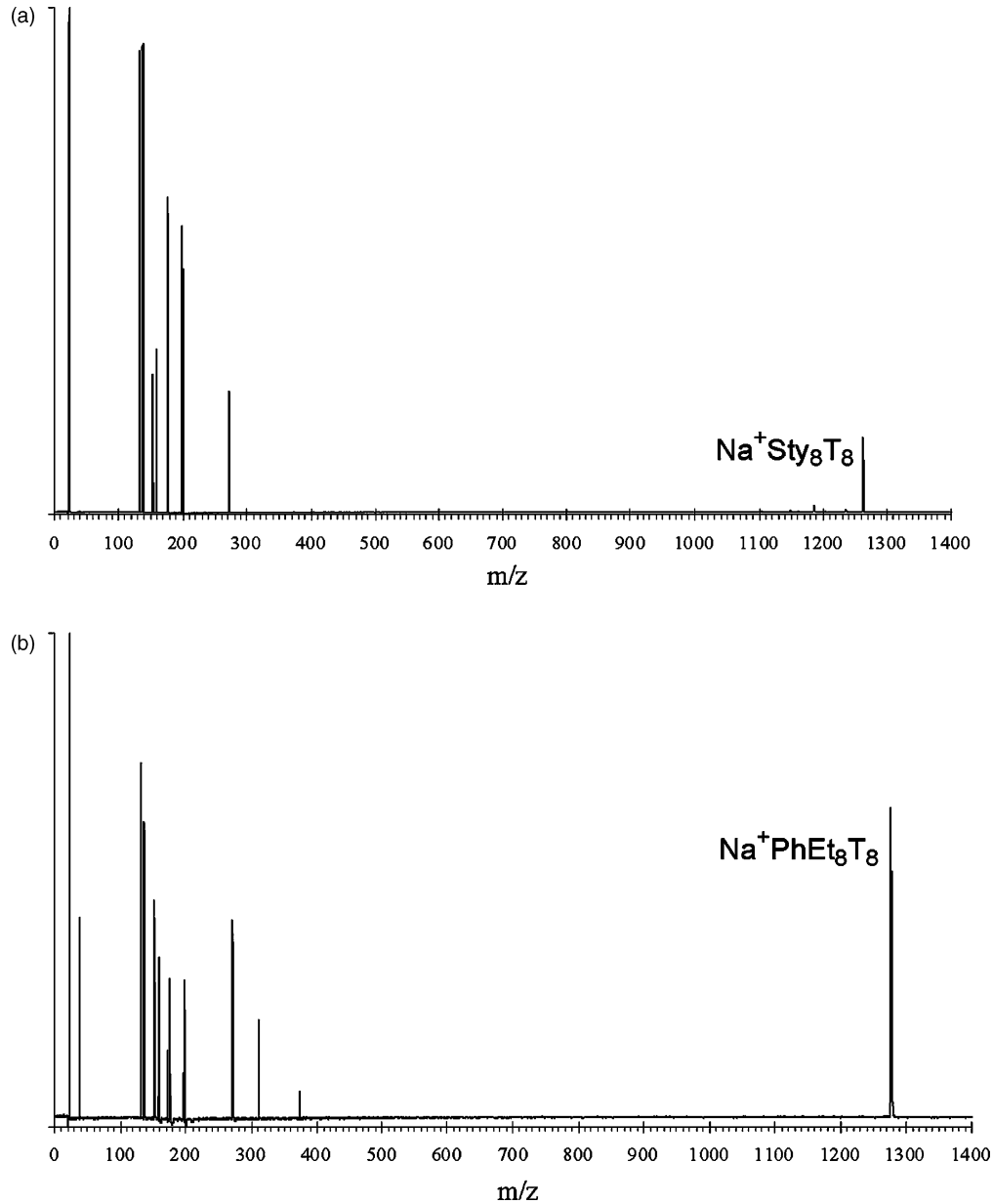

Fig. 2. MALDI-TOF mass spectra of (a) Sty_8T_8 and (b) $PhEt_8T_8$ cationized by sodium. The cluster of peaks below *m/z* 400 is due to the salt and matrix.

injection energy (300–500 eV). Thus, the relative intensities of the five ATD peaks should be accurate representations of the relative abundance of each conformer produced in the MALDI source. Collision cross-sections of each conformer can be extracted from the ATDs using Eqs. (1) and (2) (see ref. [8] for typical t_A vs. p/V plots). These values are given in Table 1.

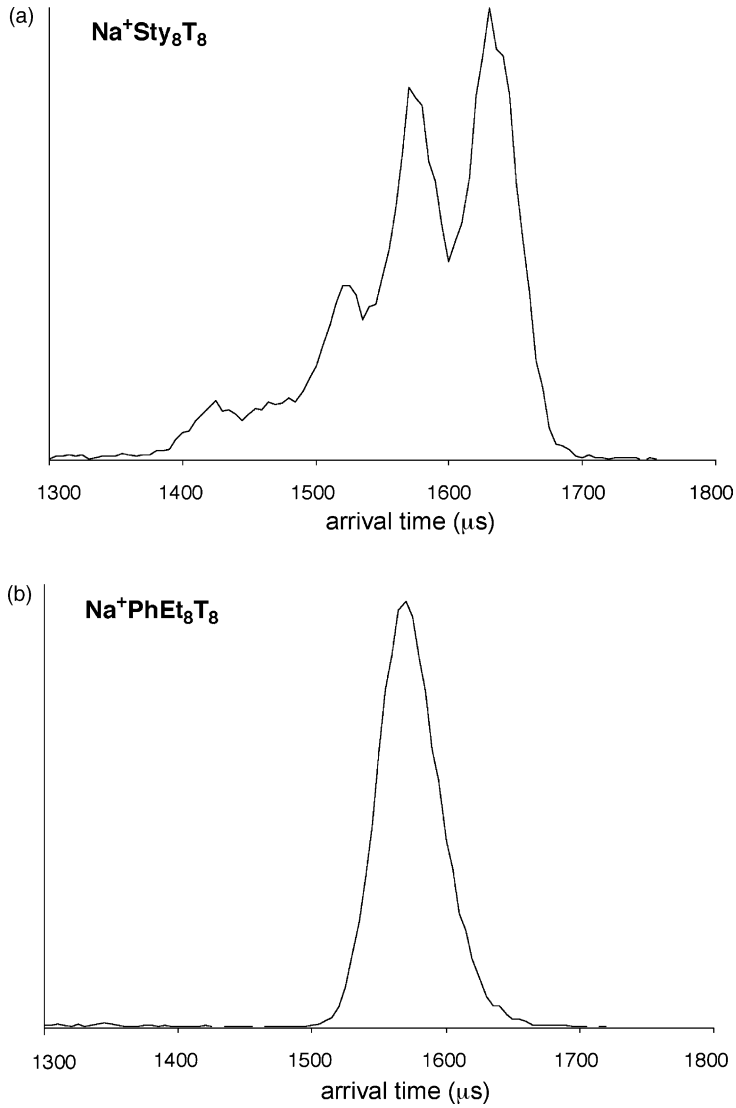

Fig. 3. ATDs of (a) $Na^+Sty_8T_8$ and (b) $Na^+PhEt_8T_8$ obtained at a drift cell temperature of 300 K. Multiple peaks in ATDs indicate the presence of multiple conformations with different collision cross-sections (and hence different arrival times).

Also shown in Table 1 is the calculated cross-section of neutral Sty_8T_8 whose structure was determined by X-ray crystallography [19]. In this structure, shown in Fig. 4, four styryl groups extend away from the Si–O cage and are ∼10 Å away from their nearest styryl neighbors. The other four styryl groups also extend away from the Si–O cage but interact with a nearest neighbor (i.e., are ∼5 Å away from each other), forming two distinct "pairs." These pairs are shown in blue in Fig. 4. The cross-section of this X-ray structure (341 $Å^2$) matches the largest of the five experimental cross-sections obtained from the ATD (340 $Å^2$).

Candidate structures of the $Na^+Sty_8T_8$ ions were generated using the theoretical methods described in the previous section. A simulated annealing/energy minimization cycle was used to produce 100 low-

Table 1
Collision cross-sections (Å^2) for $Na^+Sty_8T_8$ and $Na^+PhEt_8T_8$

Name	X-ray	Experiment	Theory
Sty_8T_8	341	340	338[a]
		330	328[b]
		324	320[c]
		310	307[d]
		293	295[e]
$PhEt_8T_8$		266	267

[a] Calculated average cross-section for "2-pair" family.
[b] Calculated average cross-section for "3-pair" family.
[c] Calculated average cross-section for "4-pair" family.
[d] Calculated average cross-section for one "*cis*" styryl group and 3 "pairs."
[e] Calculated average cross-section for two "*cis*" styryl groups and 2 "pairs."

energy structures for $Na^+Sty_8T_8$ (and $Na^+PhEt_8T_8$) and the angle averaged collision cross-section of each structure was calculated with a previously developed projection model. A "scatter plot" of cross-section vs. energy is then used to help identify the ions observed in the ATDs. The scatter plots obtained for $Na^+Sty_8T_8$ and $Na^+PhEt_8T_8$ are shown in Fig. 5. For $Na^+Sty_8T_8$ (Fig 5a), all 100 calculated structures fall within 6–7 kcal/mol of each other but three distinct families of conformers are predicted (labeled "4," "3," and "2" in the figure) that differ in the number of "pairs" of styryl groups. Examples of each family are shown in Fig. 6. In each family, the eight styryl groups extend away from the Si–O cage and the Na^+ ion coordinates to 4 oxygens on one side of the cage. The difference between the three families depends on the interactions between the styryl groups. The lowest energy structures, with the smallest cross-sections,

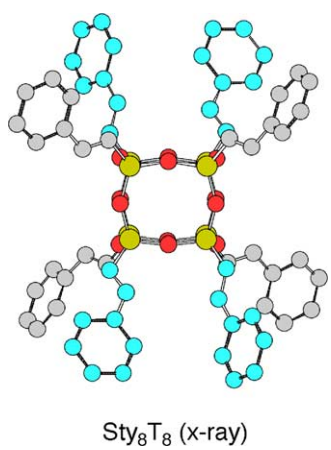

Fig. 4. X-ray structure of Sty_8T_8 (see ref. [19]). Silicon atoms are white (gold in online version), oxygens are black (red in online version), and carbons are gray (hydrogens are omitted). Styryl groups that are "paired" (within 5 Å of each other) are shown in dark gray (blue in online version).

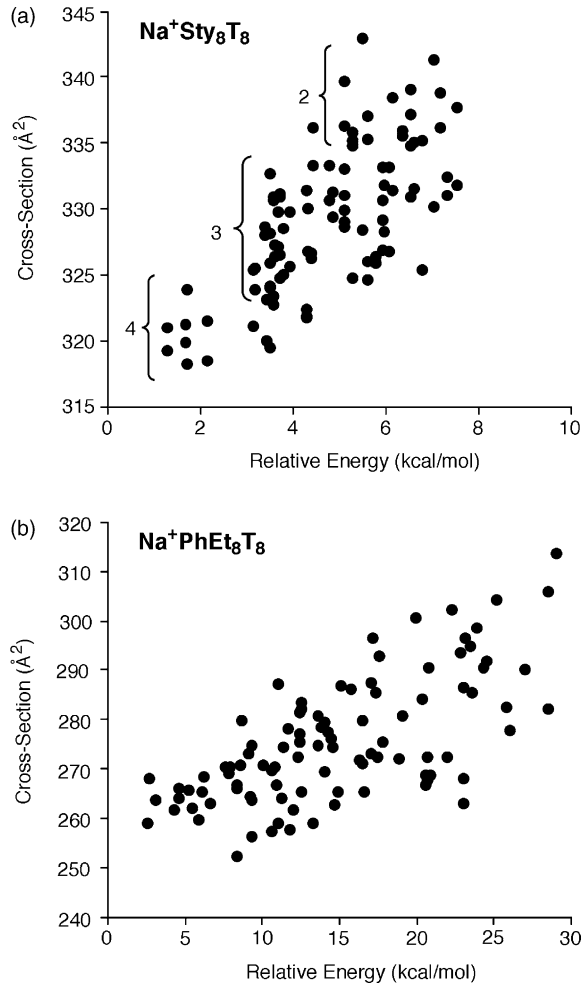

Fig. 5. Scatter plots of cross-section vs. energy for (a) $Na^+Sty_8T_8$ and (b) $Na^+PhEt_8T_8$. Each point represents one theoretical structure. For $Na^+Sty_8T_8$, three different low-energy conformers are predicted that have 2, 3, or 4 styryl "pairs" (see text and Fig. 6). For $Na^+PhEt_8T_8$, one low-energy conformation is predicted (see Fig. 8).

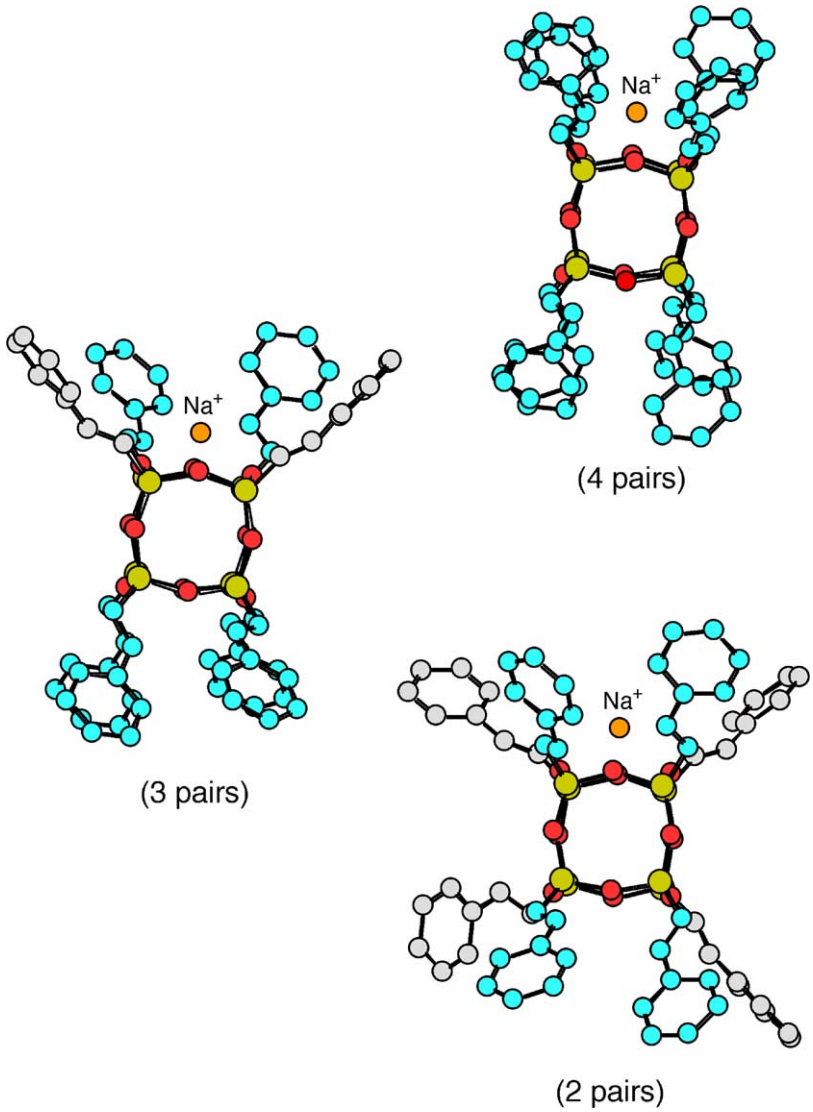

Fig. 6. Examples of the three low-energy conformers predicted for $Na^+Sty_8T_8$. Silicon atoms are white, oxygens are black, and carbons are gray (hydrogen atoms have been omitted for clarity). Styryl groups that are "paired" are shown in dark gray. (See Fig. 4 for online color key.)

have 4 "pairs" of styryl groups. That is, all eight styryl groups interact with a nearest neighbor and are ~5 Å away from it (compared to ~10 Å for styryl groups that are not paired). A given "pair," however, does not interact with any of the other three "pairs." The second family of conformers, which are ~3 kcal/mol higher in energy and have ~8 $Å^2$ larger cross-sections, have 3 "pairs" of styryl groups (shown in blue in Fig. 5). As with the lowest-energy family, a given "pair" does not interact with the other 2 "pairs." The third family of conformers, which are 5–6 kcal/mol higher in energy and have ~18 $Å^2$ larger cross-sections than the lowest-energy structures, have 2 "pairs" of styryl groups. For the "2-pair" and "3-pair" families, the relative positions of the paired styryl groups appear to be random with no noticeable energetic preferences.

The average cross-section calculated for each family of conformers is listed in Table 1. The cross-section for the "2-pair" family agrees very well with the values obtained for the X-ray structure and the largest of the five experimental cross-sections (determined from the longest time peak in the ATD). The second longest-time peak in the $Na^+Sty_8T_8$ ATD (with the second largest cross-section) can be assigned to the "3-pair" family and the middle peak in the ATD can be assigned to the "2-pair" family. This leaves two small peaks in the ATD (at shortest times) that are unaccounted for in the scatter plot shown in Fig. 5a. If, however, one or more of the styryl groups is modified then the smallest two peaks in the ATD can be accounted for by theory.

In the X-ray structure and the calculated structures shown in Fig. 6, the eight styryl groups are identical to each other in that the phenyl groups are "*trans*" with respect to the Si atom on the cage, resulting in a Si–C=C–C dihedral angle of 180°. Fig. 7, however, shows the lowest energy structures calculated for $Na^+Sty_8T_8$ in which one (Fig. 7a) and two (Fig. 7b) styryl groups are modified by rotating the phenyl groups around the C=C double bond so that they are "*cis*" with respect to the Si atom on the cage, resulting in a Si–C=C–C dihedral angle of 0° (shown in green in Fig. 7). The "*cis*" styryl group(s) folds toward the Si–O cage, rather than extending away from it like the others, and interacts with the Na^+ ion. If one styryl group is changed to "*cis*" and the remaining styryl groups form 3 "pairs" (Fig. 7a), the resulting cross-section of the structure (307 ± 3 Å^2) matches the experimental cross-section determined from the second shortest-time peak in the ATD (310 ± 3 Å^2) as shown in Table 1. If two styryl groups are changed to "*cis*" (either nearest neighbors as shown in Fig. 7b or on opposite corners of the Si–O cage) and the other styryl groups form 2 "pairs," the resulting cross-section (295 ± 3 Å^2) matches the experimental value determined for the shortest-time peak in the ATD (293 ± 3 Å^2). If the two "*cis*" styryl groups are placed on opposite sides of the Si–O cage, the remaining styryl groups cannot form multiple "pairs" and the resulting cross-section of the structure is 304 ± 3 Å^2.

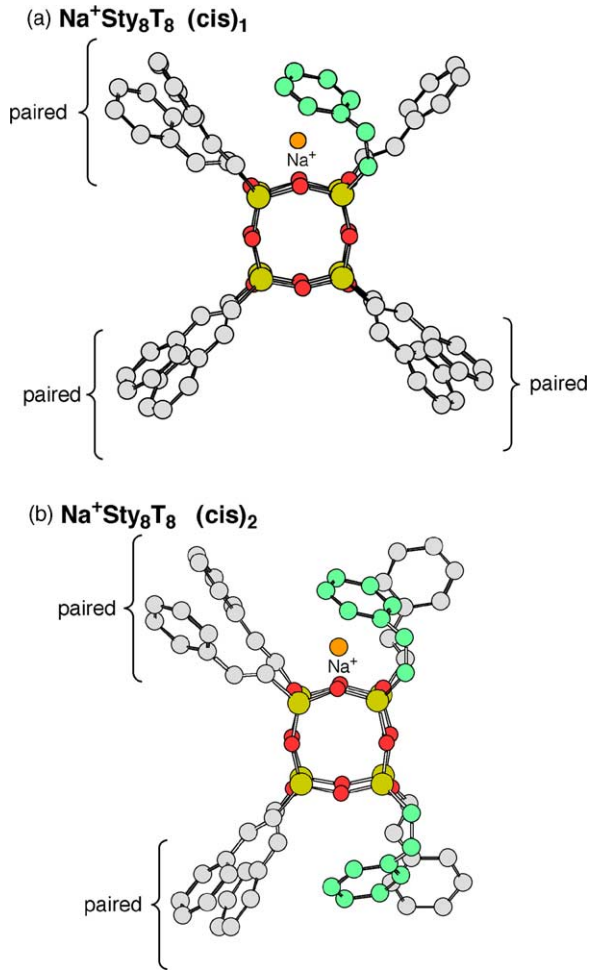

Fig. 7. Lowest energy structures calculated for $Na^+Sty_8T_8$ in which (a) one and (b) two styryl groups have been rotated so that the phenyl groups are "*cis*" with respect to the Si–O cage (Si–C=C–C dihedral angle is 0° instead of 180°). Silicon atoms are white (gold in online version), oxygens are black (red in online version), carbons are gray, and the Na^+ ion is white (orange in online version) (hydrogens have been omitted). The "*cis*" styryl groups are shown in dark gray (green in online version).

Changing a styryl group to "*cis*" costs ~5 kcal/mol, regardless of where they are positioned on the Si–O cage, so these structures are predicted to be higher in energy than those shown in Fig. 6. These "*cis*-modifications" most likely occur in the synthesis of Sty_8T_8 rather than during the ion mobility experiments since changes in injection energy did not affect

the ATD. The relative intensities of the ATD peaks indicate that these "*cis*" conformers comprise about 11% of the total Sty_8T_8 sample. Ion mobility has also been used to identify *cis* "defects" across vinyl linkages in oligophenylvinylenes [20], important optoelectronic molecules. The ability to determine such structural impurities is one of the major strengths of the ion mobility method.

One final comment about $Na^+Sty_8T_8$ concerns the relative intensities of the ATD peaks. Theory predicts that the most compact conformers, with 4 "pairs," are the lowest energy structures and the least compact conformers, with only 2 "pairs," are the highest energy structures. Yet, the $Na^+Sty_8T_8$ ATD indicates that the "2-pair" conformers are the most abundant structures with a gradual drop off in abundance as the structures become more compact. The two smallest peaks in the ATD (at shortest arrival times) have been assigned to structural "impurities" and so it is not surprising that they are the least intense peaks in the ATD. The relative intensities of the other three ATD peaks, however, seem counterintuitive from an energetic viewpoint. However, these relative peak intensities are in semi-quantitative agreement with a statistical pairing of the styryl groups. The number of ways to form 2 pairs of styryl groups (assuming nearest neighbors only) is larger than the number of ways to form 3 pairs or 4 pairs. Statistical analysis yields a ratio of the number of ways to form 2 pairs, 3 pairs, or 4 pairs as 2.3:2:1. The ratio of the ATD peak intensities assigned to the 2-pair, 3-pair, and 4-pair conformers is 2.6:2.2:1.

The energy differences predicted for the three $Na^+Sty_8T_8$ conformers are minor (±2 kcal/mol between each successive family) and it is possible that AMBER is not predicting the correct energetic trend (although most systems studied by our ion mobility/molecular modeling methods indicate that the lowest energy structures are usually the most compact). However, it may also be possible that the $Na^+Sty_8T_8$ ions pick up enough energy during the MALDI process that they can easily isomerize between the three conformers and so the distribution of each conformer is governed more by statistics than minor energy variations. Entropy can play a factor as well and most certainly favors the "2-pair" family. In any case, the energetic differences between the three conformers do not appear to significantly alter the relative abundance of each conformer.

3.2. $Na^+PhEt_8T_8$

Unlike $Na^+Sty_8T_8$, only one peak appears in the 300 K ATDs obtained for $Na^+PhEt_8T_8$ (see Fig. 3b). Single, symmetric peaks on ATDs generally indicate that either one family of conformers is present or multiple conformers are present that rapidly interconvert in the drift cell. A single peak also appears in the $Na^+PhEt_8T_8$ ATD measured at a drift cell temperature of 120 K (which should be a low enough temperature to slow down most isomerization processes and separate multiple conformers [21,22]). Hence, $Na^+PhEt_8T_8$ most likely has a single conformation in the gas phase. The experimental collision cross-section for $Na^+PhEt_8T_8$, obtained from the 300 K ATDs, is listed in Table 1.

An X-ray structure of $PhEt_8T_8$ was not available but theoretical structures for $Na^+PhEt_8T_8$ were generated using the simulated annealing cycle described previously. The resulting scatter plot of cross-section vs. energy for the 100 low-energy candidate structures of $Na^+PhEt_8T_8$ is shown in Fig. 5b. In this case, the 100 calculated structures have a 30-kcal/mol energy range instead of the 8-kcal/mol range observed for $Na^+Sty_8T_8$. The phenylethyl groups are significantly more flexible than their styryl counterparts and so a greater number of structures and corresponding energies are possible for $Na^+PhEt_8T_8$. However, as opposed to $Na^+Sty_8T_8$ in which three different low-energy conformers were predicted by theory, only one family of low-energy conformers is predicted for $Na^+PhEt_8T_8$. The lowest 5-kcal/mol structures are very similar to each other and a representative of these structures is shown in Fig. 8. Unlike the styryl groups, the phenylethyl groups actually fold toward the Si–O cage rather than extend away from it. The Na^+ ion also shifts over to one side and binds to just one oxygen atom on the Si–O cage instead of four as in $Na^+Sty_8T_8$ but is also sandwiched between two phenyl groups.

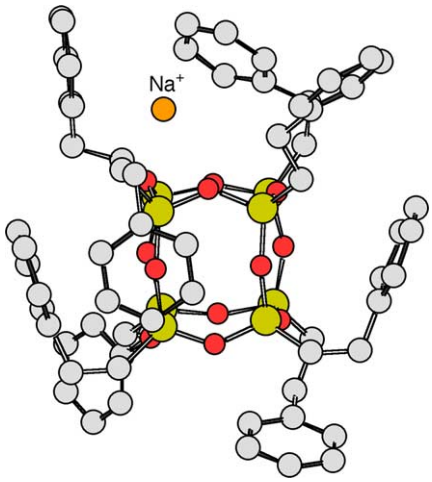

Fig. 8. Example of the lowest energy structures predicted for $Na^+PhEt_8T_8$. Silicon atoms are white, oxygens are black, carbons are gray and the Na^+ ion is white (hydrogens are omitted for clarity). (See Fig. 7 for online version color key.)

The average cross-section of the lowest 5 kcal/mol structures (267 ± 3 Å^2) was used for comparison to experiment and is listed in Table 1. This theoretical value agrees very well with the experimental cross-section obtained from the ATDs. (To account for any thermal motion $Na^+PhEt_8T_8$ may undergo during the ion mobility experiments, several low energy structures were chosen for molecular dynamics simulations at 300 K. The dynamics were run for 1000 ps and every 1 ps the resulting structure was saved and its cross-section calculated. These simulations also yielded an average cross-section of 267 Å^2, the value given in Table 1.)

One interesting point about the phenyleythyl POSS system is that it is significantly more compact than its styryl counterpart. The cross-section of $Na^+PhEt_8T_8$ is up to 30% smaller than that of $Na^+Sty_8T_8$. This is a rather large change considering that both systems have a rigid Si_8O_{12} core and only differ by a single bond (CH_2–CH_2 vs. CH=CH). This level of size difference may have serious implications if these POSS compounds are polymerized or incorporated into other polymeric systems.

The reason for the size discrepancy is clearly shown in Figs. 6 and 8. The styryl groups basically have two rigid sections while the phenylethyl groups have only one. For Sty_8T_8, the styryl groups are attached to the Si–O cage by a rigid CH=CH group. Not only does this vinyl group have a limited range of movement itself, it also hinders the movement of the phenyl rings. Hence, the styryl groups have only one option: extend away from the Si–O cage. The phenylethyl groups, on the other hand, are attached to the Si–O cage by a fairly flexible CH_2–CH_2 group. Thus, the phenylethyl groups can bend and rotate more freely than their styryl counterparts and essentially wrap around the Si–O cage. It is interesting to note that if a styryl group is attached to the Si–O cage in a *cis* rather than *trans* configuration it will fold toward the Si–O cage, similar to the phenylethyl groups, yielding a more compact structure (see Fig. 7).

4. Summary

Ion mobility experiments and molecular modeling calculations were used to determine the gas-phase conformations of sodiated POSS compounds capped with styryl and phenylethyl groups. Five resolvable conformations of $Na^+Sty_8T_8$ were observed in the ion mobility experiments. Theory predicts three low-energy families of conformers based on the relative positions of the styryl groups. In each case, the Na^+ ion is bound to four oxygens on the Si–O cage and the styryl groups extend away from the cage but the styryl groups can form two, three, or four distinct "pairs" (i.e., are within 5 Å of each other), yielding three different conformations with different collision cross-sections. The calculated cross-sections of these three conformers are in excellent agreement with the largest three experimental values. Two higher energy but more compact families of conformers are predicted by theory if one or two of the styryl groups are rotated so that the phenyl groups are "*cis*" with respect to the Si–O cage (i.e., the Si–C=C–C dihedral angle changes from 180 to 0°). The calculated cross-sections of these "*cis*" conformers agree very well with the smallest two experimental values and indicate they account for about 11% of the Sty_8T_8 sample. Only one conforma-

tion of $Na^+PhEt_8T_8$ is observed in the ion mobility experiments, a result consistent with theory. In this case, the Na^+ ion binds to one oxygen on the Si–O cage and is sandwiched between two phenyl groups. Unlike the styryl groups, the more flexible phenylethyl groups fold toward the Si–O cage, yielding a significantly more compact structure with a cross-section up to 30% smaller than that of $Na^+Sty_8T_8$.

Acknowledgements

The support of the Air Force Office of Scientific Research under grant F49620-99-1-0048 is gratefully acknowledged. We also thank Dr. Tim Haddad for providing samples and X-ray structures.

References

[1] J.D. Lichtenhan, in: J.C. Salamone (Ed.), Polymeric Materials Encyclopedia, CRC Press, New York, 1996, p. 7769.
[2] J.J. Schwab, J.D. Lichtenhan, Appl. Organometal. Chem. 12 (1998) 207.
[3] J.D. Lichtenhan, Y. Otonari, M.J. Carr, Macromolecules 28 (1995) 4355.
[4] F.J. Feher, J.J. Schwab, D.M. Tellers, A. Burstein, Main Group Chem. 2 (1998) 123.
[5] T.S. Haddad, J.D. Lichtenhan, Macromolecules 29 (1996) 234.
[6] M.T. Bowers, P.R. Kemper, G. von Helden, P.A.M. van Koppen, Science 260 (1993) 1446.
[7] D.E. Clemmer, M.F. Jarrold, Mass Spectrom. Rev. 32 (1997) 577.
[8] J. Gidden, P.R. Kemper, E. Shammel, D.P. Fee, S. Anderson, M.T. Bowers, Int. J. Mass Spectrom. 222 (2003) 63.
[9] E.A. Mason, E.W. McDaniel, Transport Properties of Ions in Gases, Wiley, New York, 1988.
[10] D.A. Case, D.A. Pearlman, J.W. Caldwell, T.E. Cheatham III, W.S. Ross, C.L. Simmerling, T.A. Darden, K.M. Merz, R.V. Stanton, A.L. Cheng, J.J. Vincent, M. Crowley, V. Tsui, R.J. Radner, Y. Duan, J. Pitera, I. Massova, G.L. Seibel, U.C. Singh, P.K. Weiner, P.A. Kollman, AMBER 6.0, University of California, San Francisco, 1999.
[11] T. Wyttenbach, G. von Helden, M.T. Bowers, Int. J. Mass Spectrom. Ion Process. 165/166 (1997) 377.
[12] J. Gidden, A.T. Jackson, J.H. Scrivens, M.T. Bowers, Int. J. Mass Spectrom. 188 (1999) 121.
[13] J. Gidden, T. Wyttenbach, J.J. Batka, P. Weis, A.T. Jackson, J.H. Scrivens, M.T. Bowers, J. Am. Soc. Mass Spectrom. 10 (1999) 883.
[14] J. Gidden, T. Wyttenbach, A.T. Jackson, J.H. Scrivens, M.T. Bowers, J. Am. Chem. Soc. 122 (2000) 4692.
[15] J. Gidden, A.T. Jackson, J.H. Scrivens, M.T. Bowers, J. Am. Soc. Mass Spectrom. 13 (2002) 499.
[16] H. Sun, D. Rigby, Spectrochim. Acta A 53 (1997) 1301.
[17] G. von Helden, M.T. Hsu, N. Gotts, M.T. Bowers, J. Phys. Chem. 97 (1993) 8182.
[18] T. Wyttenbach, G. von Helden, J.J. Batka Jr., D. Carlat, M.T. Bowers, J. Am. Soc. Mass Spectrom. 8 (1997) 275.
[19] X-ray Crystallography Data was Acquired from Dr. Tim Haddad at ERC Inc., Air Force Research Laboratory.
[20] M.A. Summers, P.R. Kemper, J.E. Bushnell, M.R. Robinson, G.C. Bazan, S.K. Buratto, M.T. Bowers, J. Am. Chem. Soc., in press.
[21] J. Gidden, T. Wyttenbach, J.J. Batka, P. Weis, A.T. Jackson, J.H. Scrivens, M.T. Bowers, J. Am Chem. Soc. 121 (1999) 1421.
[22] J. Gidden, M.T. Bowers, Eur. Phys. J. D 20 (2002) 409.